arXiv:1610.01350v2 [nucl-th] 1 Jan 2017

Chiral potential renormalized in harmonic-oscillator space

C.-J. Yang[1]

[1]*Institut de Physique Nucleaire, IN2P3-CNRS,*

Universite Paris-Sud, F-91406 Orsay Cedex, France[*]

(Dated: January 3, 2017)

Abstract

We renormalize the chiral effective field theory (EFT) potential in harmonic-oscillator (HO) model space. The low energy constants (LECs) are utilized to absorb not just the ultra-violet part of the physics due to the cutoff, but also the infrared part due to the truncation of model space. We use the inverse J-matrix method to reproduce the nucleon-nucleon (NN) scattering phase shifts in the given model space. We demonstrate that by including the NLO correction, the nucleon-nucleon scattering in the continuum could be well reproduced in the truncated HO trap space up to laboratory energy $T_{lab} = 100$ MeV with number of HO basis n_{max} as small as 10. A perturbative power counting starts at subleading order is adopted in this work, and how to extract the perturbative contribution is demonstrated. Our work serves as the input to perform ab-initio calculations.

[*]Electronic address: yangjerry@ipno.in2p3.fr

I. INTRODUCTION

With the development of computational power and technique, the input of ab-initio calculation—NN interaction—has became the one of the main uncertainties in the few- and many-body calculations. Due to the fact that calculations needed to be performed within a model space, an effective and model-independent NN potential which converges fast enough within the model space is required. Except for Fadeev-like approaches and, e.g., the Monte-Carlo techniques and in general ab initio nuclear reaction approaches that use wave functions with proper boundary conditions—which only involves the ultraviolet cutoff—the model space is usually truncated in both the ultraviolet (Λ) and infrared (λ) scales. Therefore, before trusting the results one has to check carefully the convergent pattern with respect to Λ and λ.

In the past two decades, interaction deduced from effective filed theory (EFT)[1–10] has been developed and significant efforts has been spent on the goal of providing good and model-independent description of data. The bare NN interaction obtained in the continuum cannot be directly applied into few- or many-body calculation since: (a) The model space to perform calculations usually contains both ultraviolet and infrared cutoffs. (b) Ultraviolet cutoff of the bare potential is too hard[1]. One common treatment is to perform an unitary transformation (such as Lee-Suzuki or similarity renormalization group (SRG)) to generate effective interactions from the bare one[11]. However, in addition to loosing some level of resolution—which is unavoidable when model space is reduced—the unitary transformation also generates at least one additional scale, such as the SRG flow parameter and the induced higher body force. Since the EFT power counting is usually organized in the continuum with respect to Λ alone, those extra cutoffs (due to λ and other additional scales from unitary transformation) could in principle destroy the power counting after the transformation. Without a complete check, the interaction serves as input will lose its model independent feature.

It is therefore desirable to build the effective interactions within a limited number of basis in an alternative way. The philosophy of present work is that, instead of renormalizing the interaction in the continuum first and transforming it into a given model space later, hoping to find a method of truncation (along with certain conditions) which does not affect the model-independent feature of the original interaction, one performs the renormalization directly in a given model space by

[1] The bare potential usually has an ultraviolet cutoff which is too high for the results to converge within the limited number of basis.

utilizing the low energy constants (LECs) in the EFT.

This direction has been advocated by the Arizona group [12–18], where the pionless potential is direct renormalized in a given HO space with or without a physical trap. The use of the physical trap allows one to connect the phase shifts (δ) to eigenvalues of matrix element by Busch formula[19, 20]. Similar applications to bosonic system is carried out in Ref.[21]. An alternative approach is to adopt the J-matrix formalism to relate δ to the eigenvalues[22]. Finally, an approach which deduces the potential through Bloch-Horowitz equation—the HO-based effective theory (HOBET)—is also explored[23, 24].

In this work the harmonic oscillator (HO) basis is adopted. We construct the chiral EFT interaction directly in a given model space without the HO trap. Similar to Ref.[22], the renormalization of the EFT interaction under the given infrared cutoff λ and ultraviolet cutoff Λ is done through the inverse scattering J-matrix method[25–27], which enables a direct connection between the eigenstates in truncated HO space to the NN scattering phase shifts. The truncated model space is characterized by an ultraviolet cutoff $\Lambda \sim \sqrt{M(N_{max}+3/2)\hbar\omega}$ and an infrared cutoff $\lambda \sim \sqrt{\frac{M\omega}{4(N_{max}+7/2)}}$. Here M is the nucleon mass, $N_{max} = 2n_{\max} + l$, with $n_{\max}$ the maximum number of shells included in the calculation and l the angular momentum quantum number, ω is the oscillator frequency associated with the HO basis used. Note that under the condition that the ultraviolet cutoff is saturated, detail studies in Refs.[28–30] suggest that $\lambda = \sqrt{\frac{M\omega}{4(N_{max}+7/2)}}$ should be adopted, and $\Lambda = \sqrt{M(N_{max}+7/2)\hbar\omega}$. A comparison between a more conservative definition $\lambda = \sqrt{M\hbar\omega}$ and $\lambda = \sqrt{\frac{M\omega}{4(N_{max}+7/2)}}$ can be found in Ref.[31]. For the purpose of our discussion here, the exact form of the infrared cutoff does not play a significant role. The main advantage of our approach is that the truncation is only controlled by two scales (λ, Λ), and this allows a straight forward renormalization group analysis. Moreover, recent studies[10, 32] suggest that the subleading chiral potential cannot be included non-perturbatively, if one requires the result to be renormalization group (RG) invariant. Therefore, in this work we adopt the new power counting[38–40] which treats the subleading order potential perturbatively and indicate how the perturbative treatment of chiral potential can be applied in few- and many-body calculations. Note that although the exact power counting in chiral EFT at NN sector is still an open question, our method can be applied to any arrangement of power counting.

The structure of the present work is as follows. In section II, we introduce the inverse J-matrix method. In section III, we apply the J-matrix method to the renormalization of the leading order chiral EFT potential. In section IV, we apply chiral EFT potential up to NNLO and show how to extract its perturbative contribution. Finally, we summarize our findings in section V.

II. J-MATRIX METHOD

The J-matrix method was initially derived in atomic physics[33], and later in nuclear physics using harmonic oscillator basis[34, 35]. The main idea is to expression the asymptotic scattering wavefunction in terms of infinite series of a chosen basis. In the following we just provide the necessary formula used in our calculation. A more detail derivation can be found in Ref.[25].

The Schrödinger equation reads:

$$H\Psi = (-\frac{\nabla^2}{2\mu} + V)\Psi = E\Psi. \tag{1}$$

Here $\mu = M/2$ is the reduced mass of the NN system and V represents the NN potential.

After partial-wave decomposition, the radial part of wavefunction can be expanded in HO basis:

$$\Psi_l(r) = \frac{u_l(r)}{r} = \sum_{n=0}^{n_{max}} c_{nl}\phi_{nl}(r). \tag{2}$$

Here l denotes the angular momentum quantum number, c_{nl} are constants and we have truncated the model space to $n_{\max}$ shells. The HO wavefunction $\phi_{nl}(r)$ reads

$$\phi_{nl}(r) = (-1)^n[2\pi\Gamma(l+3/2)]^{-1/2}b^{-3/2}[L_n^{(l+1/2)}(0)]^{-1/2}(\frac{r}{b})^l \exp[-\frac{r^2}{2b^2}]L_n^{(l+1/2)}(\frac{r^2}{b^2}), \tag{3}$$

with $b = \frac{1}{\sqrt{\mu\omega}}$, $L_n^{(\alpha)}$ the generalized Laguerre polynomial. $\phi_{nl}(r)$ satisfies

$$\begin{aligned}
\int_0^\infty \phi_{nl}^2(r)4\pi r^2 dr &= 1, \\
(2n+l+\frac{3}{2})\omega &= \int_0^\infty \phi_{nl}(r)[\frac{1}{2\mu}(-\frac{1}{r}\frac{d^2}{dr^2}r + \frac{l(l+1)}{r^2}) + \frac{1}{2}\mu r^2\omega^2]\phi_{nl}(r)4\pi r^2 dr.
\end{aligned}$$

The maximum accessible energy in the model space is characterized by the ultraviolet cutoff $\Lambda = \sqrt{M(2n_{max}+l+3/2)\hbar\omega}$.

The kinetic energy under HO basis reads

$$T_{n,n-1}^l = -\frac{1}{2}\sqrt{n(n+l+1/2)}, \tag{4}$$

$$T_{n,n}^l = \frac{1}{2}(2n+l+3/2), \tag{5}$$

$$T_{n,n+1}^l = -\frac{1}{2}\sqrt{(n+1)(n+l+3/2)}, \tag{6}$$

$$T_{n,m}^l = 0 \text{ (for } |n-m| \geq 2). \tag{7}$$

For the potential, we adopt the momentum space form, and one has

$$V_{ll'}(r,r') = \frac{2}{\pi}\int_0^\infty k^2 dk \int_0^\infty p^2 dp j_l(kr)V_{ll'}(k,p,\Lambda)j_{l'}(pr'), \tag{8}$$

where $l(l')$ represents the angular momentum quantum numbers. The momentum space potential is given by

$$V_{ll'}(k,p,\Lambda) = \left[V_{ll'}^{LR}(k,p) + V_{ll'}^{SR}(k,p)\right] R(k,p,\Lambda), \tag{9}$$

where the superscript LR (SR) denotes the long- (short-) range part of the potential. $R(k,p,\Lambda)$ is a regulator, and in this work we adopt

$$R(k,p,\Lambda) = \exp(-\frac{p^4+k^4}{\Lambda^4}). \tag{10}$$

Once the coordinate space representation $V_{ll'}(r,r')$ is obtained, the matrix element of Hamiltonian $H_{ll'}$ reads:

$$\langle H_{ll'}\rangle_{nm} = T_{n,m}^{ll'} + \int_0^\infty 4\pi r^2 dr \int_0^\infty 4\pi r'^2 dr' \phi_{nl}(r) V_{ll'}(r,r') \phi_{ml'}(r'), \tag{11}$$

with

$$T_{n,m}^{l\neq l'} = 0. \tag{12}$$

Moreover, due to the special property of the HO potential, one can further simplify the above equation into:

$$\begin{aligned} \langle H_{ll'}\rangle_{nm} &= T_{n,m}^{ll'} + \frac{2}{\pi}\int_0^{\Lambda_c} k^2 dk \int_0^{\Lambda_c} p^2 dp \phi_{nl}(k) V_{ll'}(k,p,\Lambda) \phi_{ml'}(p) & (13)\\ &= T_{n,m}^{ll'} + V_{n,m}^{ll'}, & (14) \end{aligned}$$

where $\phi_{nl}(k)$ has the same form as $\phi_{nl}(r)$, with r replaced by k and $b = \sqrt{\mu\omega}$. The energy spectrum, E_n, can be obtained by diagonalizing $H_{ll'}$ (for coupled-channels, all possible ll' need to be included). Note that although the regulator $R(k,p,\Lambda)$ alone is sufficient for the integral to converge, we also impose an additional sharp cutoff Λ_c (which is set to $\Lambda_c = \Lambda + 200$ MeV throughout this work) in Eq. (13) just to reduce the numerical task. The ultraviolet property of the potential is majorly determined by the intrinsic cutoff Λ.

The key of connecting the NN scattering phase shifts to E_n is to evaluate the potential $< V_{ll'} >_{nm}$ up to $n = m = n_{max}$, but keep the size of kinetic part to infinity. Then formula connecting the asymptotic wavefunction to scattering phase shift can be shown to have the following form:

$$\tan\delta(E) = -\frac{S_{n_{max}l}(E) - G_{n_{max}n_{max}} T^l_{n_{max},n_{max}+1} S_{n_{max}+1,l}(E)}{C_{n_{max}l}(E) - G_{n_{max}n_{max}} T^l_{n_{max},n_{max}+1} C_{n_{max}+1,l}(E)}, \tag{15}$$

with

$$S_{nl}(E) = \sqrt{\frac{\pi b n!}{\Gamma(n+l+3/2)}}(\frac{2E}{\omega})^{\frac{l+1}{2}}\exp[-\frac{E}{\omega}]L_n^{l+1/2}(\frac{2E}{\omega}), \tag{16}$$

$$C_{nl}(E) = \sqrt{\frac{\pi b n!}{\Gamma(n+l+3/2)}}\frac{(\frac{2E}{\omega})^{-l/2}}{\Gamma(-l+1/2)}\exp[-\frac{E}{\omega}]\Phi(-n-l-1/2,-l+1/2;\frac{2E}{\omega}), \tag{17}$$

$$G_{nn'} = -\sum_{\lambda'=0}^{n_{max}}\frac{\langle n|\lambda'\rangle\langle\lambda'|n'\rangle}{E_{\lambda'}-E}. \tag{18}$$

Here $\Phi(a,b;z)$ is the confluent hypergeometric function of 1^{st} kind, $\langle n|\lambda'\rangle$ and $E_{\lambda'}$ are eigenvector and eigenvalues of the Hamiltonian $\langle H_{ll'}\rangle_{nm}$ truncated up to $n=m=n_{max}$.

For cases where two partial-waves with the same total angular momentum quantum number J couple together, the number of basis increase to $N_{\max}=n^s_{\max}+n^d_{\max}+1$[2]. Note that here we have labelled the two channels as s ($l=J-1$) and d ($l=J+1$) here. Define

$$\varsigma_{\Gamma\Gamma'} = -\sum_{\lambda'=0}^{N_{max}}\frac{\langle n^{\Gamma}_{\max}|\lambda'\rangle\langle\lambda'|n^{\Gamma'}_{\max}\rangle}{E_{\lambda'}-E}, \tag{19}$$

where $\langle n^{\Gamma^{(\prime)}}_{\max}|\lambda'\rangle$ is the $\Gamma^{(\prime)}-$wave component of the eigenvector. Then the relation analog to Eq. (15)-(18) can be obtained by solving the following equations,

$$\varsigma_{ss} = \frac{\Delta_{ss}(E)}{T^s_{N_s,N_s+1}\Delta(E)}, \tag{20}$$

$$\varsigma_{dd} = \frac{\Delta_{dd}(E)}{T^d_{N_d,N_d+1}\Delta(E)}, \tag{21}$$

$$\varsigma_{sd} = \varsigma_{ds} = \frac{K_{sd}}{2T^s_{N_s,N_s+1}T^d_{N_d,N_d+1}\Delta(E)}. \tag{22}$$

$$\begin{aligned}\Delta_{ss}(E) = {} & \left[S_{n^s_{\max},s}(E)+K_{ss}(E)C_{n^s_{\max},s}(E)\right]\left[S_{n^d_{\max}+1,d}(E)+K_{dd}(E)C_{n^d_{\max}+1,d}(E)\right]\\ & -K^2_{sd}(E)C_{n^s_{\max},s}(E)C_{n^d_{\max}+1,d}(E),\end{aligned} \tag{23}$$

$$\begin{aligned}\Delta_{dd}(E) = {} & \left[S_{n^s_{\max}+1,s}(E)+K_{ss}(E)C_{n^s_{\max}+1,s}(E)\right]\left[S_{n^d_{\max},d}(E)+K_{dd}(E)C_{n^d_{\max},d}(E)\right]\\ & -K^2_{sd}(E)C_{n^s_{\max}+1,s}(E)C_{n^d_{\max},d}(E),\end{aligned} \tag{24}$$

$$\begin{aligned}\Delta(E) = {} & \left[S_{n^s_{\max}+1,s}(E)+K_{ss}(E)C_{n^s_{\max}+1,s}(E)\right]\left[S_{n^d_{\max}+1,d}(E)+K_{dd}(E)C_{n^d_{\max}+1,d}(E)\right]\\ & -K^2_{sd}(E)C_{n^s_{\max}+1,s}(E)C_{n^d_{\max}+1,d}(E).\end{aligned} \tag{25}$$

[2] Both s and d channel runs from 0 to $n^{s,d}_{\max}$, so $N_{\max}=n^s_{\max}+n^d_{\max}+1$.

$\mathcal{O}(1)$	OPE, $C_{^1S_0}$, $\begin{pmatrix} C_{^3S_1} & 0 \\ 0 & 0 \end{pmatrix}$, $C_{^3P_0}p'p$, $\begin{pmatrix} C_{^3P_2}p'p & 0 \\ 0 & 0 \end{pmatrix}$
$\mathcal{O}(Q)$	$D_{^1S_0}(p'^2+p^2)$
$\mathcal{O}(Q^2)$	TPE0, $E_{^1S_0}p'^2p^2$, $\begin{pmatrix} D_{^3S_1}(p'^2+p^2) & E_{\rm SD}\,p^2 \\ E_{\rm SD}\,p'^2 & 0 \end{pmatrix}$, $D_{^3P_0}\,p'p(p'^2+p^2)$, $p'p\begin{pmatrix} D_{^3P_2}(p'^2+p^2) & E_{\rm PF}\,p^2 \\ E_{\rm PF}\,p'^2 & 0 \end{pmatrix}$, $C_{^1P_1}p'p$, $C_{^3P_1}p'p$
$\mathcal{O}(Q^3)$	TPE1, $F_{^1S_0}p'^2p^2(p'^2+p^2)$

TABLE I: Power counting for pion exchanges, S and P-wave counterterms up to $\mathcal{O}(Q^3)$. p (p') is the magnitude of the center-of-mass incoming (outgoing) momentum. The two-by-two matrices are for the coupled-channels.

$$K_{ss}(E) = \frac{\tan\delta_s + \tan^2\varepsilon\tan\delta_d}{1-\tan^2\varepsilon\tan\delta_s\tan\delta_d}, \tag{26}$$

$$K_{dd}(E) = \frac{\tan\delta_d + \tan^2\varepsilon\tan\delta_s}{1-\tan^2\varepsilon\tan\delta_s\tan\delta_d}, \tag{27}$$

$$K_{sd}(E) = K_{ds}(E) = \frac{\tan\varepsilon}{\cos\delta_s\cos\delta_d(1-\tan^2\varepsilon\tan\delta_s\tan\delta_d)}. \tag{28}$$

One first obtain $\varsigma_{ss,sd,dd}$ from the eigenvalues and eigenvectors using Eq. (19), then solve for $K_{ss,sd,dd}(E)$ in Eq. (20)-(25). Finally, the phase shifts (δ_s, δ_d) and the mixing angle ε can be solved from Eq. (26)-(28).

In principle, once we have the eigenvalues and eigenvectors, the above approach allows us to obtain the phase shifts at any energy. In our approach, we adjust the LECs in our chiral potential and perform best fit of the resulting phase shifts to the Nijmegen analysis[36, 37].

III. LEADING ORDER RESULTS

The leading order potential entered in Eq. (9) is the one-pion-exchange potential (OPE). In this work we consider partial-waves $^1S_0$, $^3S_1 - ^3D_1$, $^1P_1$, $^3P_0$, $^3P_1$, $^3P_2 - ^3F_2$. The associated contact terms are listed in Table I in terms of $O(Q^n)$: the order where the final amplitude is summed up to. Note that for singular attractive P-waves ($^3P_0$, $^3P_2 - ^3F_2$), the contact terms are promoted to appear one order earlier with respect to the Weinberg power counting[1, 2]. The contact terms, when presented, are renormalized to produce best fit to the Nijmegen phase shifts at laboratory energy $T_{lab} \leq 10$ MeV. The two exceptions are the $^1S_0$ and $^3S_1 - ^3D_1$ channel, where we renormalize

to their scattering length a_0. Once renormalization is completed, we examine how well the NN scattering phase shifts could be reproduced in the truncated HO space. In Fig. 1 we plot the $^1S_0$ phase shift obtained with $n_{max} = 10 - 40$ and $\omega = 20$ MeV. The two cutoffs in Eq. (13) are set to $\Lambda_c = 800$ MeV, $\Lambda = 600$ MeV. As one can see, with the increase of n_{max}—which implies the increase of ultraviolet cutoff the decrease of the infrared cutoff λ—all of the LO phase shifts converge to those obtained by solving Lippmann-Schwinger equation in the continuum.

One feature of J-matrix method can be seen in the $n_{max} = 10$ curve in Fig.1 is the oscillatory behavior in phase shift δ. Note that here $\sqrt{M(N_{max} + 3/2)\hbar\omega} = 628$ MeV> 600 MeV. Thus, the model space's ultraviolet cutoff is already larger than the ultraviolet cutoff in the potential. However, the $n_{max} = 10$ curve shows that the matrix element is still not saturated by enough number of basis to reproduce the continuum properties at all T_{lab}. This is also observed in Ref.[22]. In general, we found that $\sqrt{M(N_{max} + 3/2)\hbar\omega} > R\Lambda$ is required to eliminate the oscillatory behavior, where R is a constant greater than 1. The exact value of R depends on the strength and form of interaction, we found that for OPE, $R \sim 2$.[3] We note that this feature is not linked to the infrared cutoff, as one can increase ω to 120 MeV and use the same n_{max}—which increase ultraviolet and infrared cutoff at the same time—to eliminate the oscillatory phase shift. This is shown by the curve with plus sign in Fig.1.

In order to have a further look of the problem, we insert a physical HO-trap ($\frac{1}{2}\mu r^2\omega^2$) into the Hamiltonian. Eq. (11) then becomes

$$\langle H_{ll'}\rangle_{nm} = T^{ll'}_{n,m} + \frac{1}{2}\mu r^2\omega^2 + \int_0^\infty 4\pi r^2 dr \int_0^\infty 4\pi r'^2 dr' \phi_{nl}(r) V_{ll'}(r,r') \phi_{ml'}(r') \quad (29)$$

$$= \delta_{ll'}\delta_{nm}(2n + l + \frac{3}{2})\omega + \int_0^\infty 4\pi r^2 dr \int_0^\infty 4\pi r'^2 dr' \phi_{nl}(r) V_{ll'}(r,r') \phi_{ml'}(r'). \quad (30)$$

Here for $V_{ll'}$ we insert the same LO potential renormalized by the J-matrix method. Then Busch formula can then be adopted to extract the phase shift. The result is presented in Fig.2. As one can see, the phase shift obtained by J-matrix method ($\delta_{J-matrix}$) oscillates around the one obtained by Busch formula (δ_{busch}). For every c.m. energy $E_{cm} \sim 2\omega$ ($T_{lab} = 2E_{cm}$), one cycle of oscillation is completed. To show this is not a coincident, we increase the intrinsic cutoffs of potential to $\Lambda_c = 1000$ MeV, $\Lambda = 800$ MeV and present the same comparison in Fig.3. Fig.2 and 3 confirm that the oscillatory phase shift given by J-matrix method is an artifact of using (not enough) HO-basis to represent continuum properties. The phase shift between the two intervals just cannot be trusted. Therefore, in J-matrix method without sufficient combination of N_{max} and

[3] We observed that the factor R increases for coupled-channels and more singular potentials.

ω, one needs to carefully choose the energies where the renormalization is performed. Otherwise, additional error would appear due to adopting un-trustable $\delta_{J-matrix}(E)$ in the renormalization procedure.

The effect of $\sqrt{M(N_{max}+3/2)\hbar\omega} < R\Lambda$ appears to be less problematic for bound-state-related properties. In Fig.4 , we compare the $^3S_1$ phase shift with the LEC fixed by the scattering length $a_0 = 5.4$ fm to the one fixed by and the deuteron binding energy $E_b = -2.225$ MeV. From the converge pattern $n_{max} = 8$ to $n_{max} = 16$, one clearly sees that the oscillation is more centralized to its final converged value ($n_{max} = 16$ curve) in the right panel of Fig.4 than in the left panel. This shows that bound state indeed acts as one of the energies where $\delta_{busch}(E) = \delta_{J-matrix}(E)$.

The role of the additonal cutoff Λ_c in Eq. (13) is just to provide the numerical definiteness. We have verified that the phase shifts presented above are almost unchanged (relative difference $< 1\%$) by replacing the above Λ_c (800 MeV or 1000 MeV) by $\Lambda_c \to \infty$.

The $^3D_1$, ε_1 and p-waves phase shifts are shown in Fig. 5. They present similar converge pattern as shown in S-waves.

In Fig. 6 and Fig. 7, we plot the phase shifts generated by LO potential with larger intrinsic cutoffs, i.e., $\Lambda_c = 1000$ MeV, $\Lambda = 800$ MeV. Here we demonstrate that by increasing $\omega = 120$ MeV, the convergence can be reached with a much lower n_{max}. This is due to that: (a) the ultraviolet part of the potential is saturated with smaller n_{max}; (b) the oscillatory behavior is reduced at the same time for larger ω. In most of the channels, $n_{max} = 8$ is enough to reach convergence. Meanwhile, the mixing angle ε_1 and those singular attractive P-waves ($^3P_0$ and $^3P_2 - ^3F_2$) require a higher $n_{max}(= 16)$ to reach convergence. Note that for $n_{max} = 8$, $\sqrt{M(N_{max}+3/2)\hbar\omega} \sim 1385$ MeV, which already exceeds the intrinsic ultraviolet cutoffs in the potential. Therefore the rate of convergence in these channels (ε_1, $^3P_0$ and $^3P_2 - ^3F_2$) appears to be more sensitive to the residue-infrared-cutoff-dependence—the remaining cutoff dependence after using contact terms to renormalize both the short- and long-range physics.

IV. PERTURBATIVE TREATMENT

A. Treatment for subleading potentials

If one follows Weinberg power counting, all potentials are added up and treated non-perturbatively. The renormalization would follow exactly the same procedure as the LO performed in the previous section. However, in order to achieve renormlization group (RG) invariant at arbi-

trary high Λ_a, it is shown that at least some of the subleading chiral potential needed to be added perturbatively[38–41]. Here we adopt the new power counting proposed in Ref.[40], with contact terms listed in Table I. Starting from next-to-leading order (NLO), the potentials are treated perturbatively. The Hamiltonian we want to solve then has the form

$$H = H_{LO} + V^{(1)} + V^{(2)} + ..., \tag{31}$$

where $H_{LO} = H_0 + V_{LO}$ is the part to be iterated to all order, and the rest $(V^{(1)} + V^{(2)} + ...)$ are to be treated as perturbation. Here the superscript denotes the order in perturbation theory where the potential enters.

The corresponding wavefunction and energy are:

$$\Psi = \Psi_{LO} + \Psi^{(1)} + \Psi^{(2)} + ..., \tag{32}$$

$$E = E_{LO} + E^{(1)} + E^{(2)} + ... \tag{33}$$

In perturbation theory one has to solve:

LO (E_{LO}):

$$(H_{LO} - E_{LO})\Psi_{LO} = 0 \tag{34}$$

NLO ($E^{(1)}$):

$$(H_{LO} - E_{LO})\Psi^{(1)} = (E^{(1)} - V^{(1)})\Psi_{LO} \tag{35}$$

NNLO ($E^{(2)}$):

$$(H_{LO} - E_{LO})\Psi^{(2)} = (E^{(2)} - V^{(2)})\Psi_{LO} + (E^{(1)} - V^{(1)})\Psi^{(1)} \tag{36}$$

However, the above is difficult to deal with, especially when the basis-state grows, as each higher order correction demands accurate information from all eigen-states at previous order. Moreover, the above procedure is difficult for the implement into few- and many-body calculation.

A better way to perform the perturbative calculation is to associate a small parameter σ^v to $V^{(v)}$,

$$H(v, \sigma) = H_{LO} + \sigma V^{(1)} + \sigma^2 V^{(2)} + ... + \sigma^v V^{(v)}, \tag{37}$$

where v denotes order of truncation. The perturbative solution, which is the one we would like to extract, is

$$E(v) = E_{LO} + E^{(1)} + E^{(2)} + ...E^{(v)}. \tag{38}$$

On the other hand, denote the full non-perturbative eigen-energy (obtained by directly diagonalizing Eq. (37) truncated at order v) by $\xi(v,\sigma)$. One can express $\xi(v,\sigma)$ as

$$\xi(v,\sigma) = E_{LO} + \sigma E^{(1)} + \sigma^2 E^{(2)} + ...\sigma^v E^{(v)} + O(\sigma^{v+1}Q^{v+1}). \tag{39}$$

Then by varying σ and diagonalizing $H(v,\sigma)$, one can extract $E^{(1,2,3,...)}$ in Eq. (38).

We note that this method is very general and can be directly applied to few- and many-body calculations without modifying the existing codes.

B. NLO and NNLO results

The NLO and NNLO phase shifts based on power counting of Ref.[40] are presented in Figs. 8-11. Here Fig. 8 and 9 are for potential with intrinsic cutoffs $\Lambda_c = 800$ MeV, $\Lambda = 600$ MeV, and Fig. 10 and 11 are for $\Lambda_c = 1000$ MeV, $\Lambda = 800$ MeV. The subleading phase shifts are obtained perturbatively according to the method introduced in section IV A. The LECs are renormalized to reproduce the Nijmegen phase shifts up to the maximum T_{lab} shown in each channel. In $^3S_1 - ^3D_1$ channel, the deuteron binding energy $E_b = -2.224$ MeV is also adopted in the fit.

Unlike the conventional Weinberg counting, where the order of chiral potential equals to the order in the final amplitude, the same dose not necessary hold for the new power counting. Denote the leading (subleading) two-pion-exchange potential as TPE0 (TPE1)[4], in most of the channels presented here, TPE0 enters at NLO and TPE1 enters at NNLO. For these cases potential up to TPE0 and TPE1 both enter as one insertion[5] in the LO wavefunction, and the resulting phase shifts are NLO and NNLO, respectively. However, when a non-vanishing O(Q) potential appears, such as in the $^1S_0$ channel, NLO contains only contact terms and TPE0 enters at NNLO. Here NNLO includes one insertion of TPE0 and two insertions[6] of the O(Q) contact term.

As one can see, with the inclusion of NLO/NNLO contribution, the phase shifts converge already at $(\omega, n_{max}) = (120, 10)$ for both of the potentials adopted here (the one with $\Lambda_c = 800$ MeV, $\Lambda = 600$ MeV and the other with $\Lambda_c = 1000$ MeV, $\Lambda = 800$ MeV). The reproduction of Nijmegen phase shifts are comparable to those obtained in the continuum[40]. For lower value of ω, i.e., $\omega = 60$ MeV, the minimum n_{max} required for the NNLO phase shifts to converge ranges from $n_{max} = 15 - 20$ depends on the channels. In general, the quality of fit we obtained are

[4] In Weinberg counting, TPE0 equals to the NLO(Q^2) and TPE1 equals to the NNLO(Q^3) potential.
[5] This means one only extracts $E^{(1)}$ in Eq. (38).
[6] This is equivalent to evaluate up to $E^{(2)}$ contribution coming from $V^{(1)}$ in Eq. (38).

comparable to those obtained by the standard Weinberg counting, with only one exception: the NNLO $^3P_1$ channel. In this case, the same behavior is observed in the continuum as well[40]. This might suggest that the $c_{1,3,4}$ adopted in TPE1 need to be re-adjusted, or an adoption of the $\Delta(1232)-$included potential is necessary in order to cure this behavior.

V. CONCLUSION

We have performed a new approach to generate the chiral EFT potential in the truncated model space. We utilize the contact interactions presented in EFT to absorb the effects coming from both ultraviolet and infrared cutoffs. The connection between eigenstate of HO-basis and NN scattering phase shift are established by the J-matrix formalism. This allows a direct evaluation of NN scattering in HO-basis without applying a physical trap. In our procedure, the RG analysis can be carried out in a straight forward way as the results depends only on two scales: the infrared cutoff λ and the ultraviolet cutoff Λ. This paves a way to provide a truly model independent procedure to perform ab-initio calculations. Also, the perturbative treatment of chiral potential is carried out in the truncated model space through a method which is directly applicable to many-body calculation.

There are many possibilities to extend the current study. In particular, the interaction obtained in this work will be applied to the 3-, 4- and many-body calculations within the no-core-shell-model framework[42].

Acknowledgments

We thank A. Shirokov, N. Barnea, D. Lee, G. Hupin, M. Grasso, B.R. Barrett T. Papenbrock, R.J. Furnstahl and U. van Kolck for useful discussions and suggestions. More importantly, the author is grateful for the valuable discussions and supports from G. Orlandini and W. Leidemann. Part of this work was carried out in Univ. of Trento under MIUR grant PRIN-2009TWL3MX.

[1] S. Weinberg, Phys. Lett. B **251**, 288 (1990).

[2] S. Weinberg, Nucl. Phys. B **363**, 3 (1991).

[3] C. Ordonez, L. Ray and U. van Kolck, Phys. Rev. Lett. **72**, 1982 (1994); Phys. Rev. **C53**, 2086 (1996).

[4] E. Epelbaum, W. Glockle and U.-G. Meissner, Nucl. Phys. A **637**, 107 (1998); Nucl. Phys. A **671**, 295 (2000).

[5] D. R. Entem and R. Machleidt, Phys. Lett. **B524**, 93 (2002); Phys. Rev. **C66**, 014002 (2002).

[6] E. Epelbaum, W. Glockle and U.-G. Meissner, Nucl. Phys. **A747**, 362 (2005).

[7] U. van Kolck, Prog. Part. Nucl. Phys. **43**, 337 (1999).

[8] P. F. Bedaque and U. van Kolck, Ann. Rev. Nucl. Part. Sci. **52**, 339 (2002).

[9] E. Epelbaum, H. W. Hammer and U. G. Meissner, Rev. Mod. Phys. **81**, 1773 (2009).

[10] A. Nogga, R.G.E. Timmermans and U. van Kolck, Phys. Rev. C **72**, 054006 (2005).

[11] S. Okubo, Prog. Theor. Phys. **12**, 603 (1954); K. Suzuki and S.Y. Lee, Prog. Theor. Phys. **64**, 2091 (1980); K. Suzuki, Prog. Theor. Phys. **68**, 246 (1982); K. Suzuki and R. Okamoto, Prog. Theor. Phys. **70**, 439 (1983).

[12] I. Stetcu, B.R. Barrett, P, Navratil, J.P. Vary, Phys. Rev. C **71**, 044325 (2005).

[13] I. Stetcu, B.R. Barrett, P, Navratil, U. van Kolck, Phys. Lett. B **653**, (2007) 358.

[14] I. Stetcu, B.R. Barrett, P, Navratil, U. van Kolck, J.P. Vary, Phys. Rev. A **76**, 063613 (2007).

[15] I. Stetcu, J. Rotureau, B.R. Barrett, U. van Kolck, J. Phys. G **37**, 064033 (2010).

[16] J. Rotureau, I. Stetcu, B.R. Barrett, M.C. Birse, U. van Kolck, Phys. Rev. A **82**, 032711 (2010).

[17] I. Stetcu, J. Rotureau, B.R. Barrett, U. van Kolck, Annals. Phys. **325**, 1644-1666 (2010).

[18] J. Rotureau, I. Stetcu, B.R. Barrett, U. van Kolck, Phys. Rev. C **85**, 034003 (2012).

[19] T. Busch, B.-G. Englert, K. Rzazewski, M. Wilkens, Found. Phys. **28**, (1998) 549; S. Jonsell, Few-body Syst. **31** (2002) 255.

[20] T. Luu, M. Savage, A. Schwenk, J.P. Vary, Phys. Rev. C **82**, 034003 (2010).

[21] S. Tolle, H.-W. Hammer and B. Ch. Metsch, Comptes Rendus Physique 12, 59 70 (2011); J. of Physics G 40, 055004 (2013).

[22] S. Binder, A. Ekstrom, G. Hagen, T. Papenbrock and K.A. Wendt, Phys. Rev. C **93** 044332 (2016).

[23] W. C. Haxton, Phys. Rev. C. **77** 034005 (2008).

[24] Kenneth S. McElvain and W.C. Haxton, arXiv:1607.06863 [nucl-th].

[25] A. M. Shirokov, A. I. Mazur, S. A. Zaytsev, J. P. Vary, and T. A. Weber, Phys. Rev. C **70** 044005 (2004); Phys. Lett. B **621** 96-101 (2005).

[26] A. M. Shirokov, J. P. Vary, A. I. Mazur, and T. A. Weber, Phys. Lett. B **644**, 33 (2007).

[27] P. Maris, J. P. Vary, and A. M. Shirokov, Phys. Rev. C **79**, 014308 (2009).

[28] S. N. More, A. Ekstrom, R. J. Furnstahl, G. Hagen, and T. Papenbrock, Phys. Rev. C **87** 044326 (2013).

[29] R. J. Furnstahl, S. N. More, and T. Papenbrock, Phys. Rev. C89 044301 (2014).

[30] S. Konig, S. K. Bogner, R. J. Furnstahl, S. N. More, and T. Papenbrock, Phys. Rev. C **90** 064007 (2014).

[31] Sidney A.Coon, Matthew I. Avetian, Michael K.G. Kruse, U. van Kolck, Pieter Maris and James P. Vary, Phys. Rev. C86 054002 (2012).

[32] C.-J. Yang, Ch. Elster and D. R. Phillips, Phys. Rev. C **80**, 034002 (2009), Phys. Rev. C **80**, 044002 (2009); Ch. Zeoli, R. Machleidt, D. R. Entem, arXiv:1208.2657 [nucl-th].

[33] H. A. Yamani, L. Fishman, J. Math. Phys., 16, 410 (1975).

[34] G. F. Filippov and I. P. Okhrimenko, Yad. Fiz. 32, 932 (1980) [Sov. J. Nucl. Phys. 32, 480 (1980)]; G. F. Filippov, Yad. Fiz. 33, 928 (1981) [Sov. J. Nucl. Phys. 33, 488 (1981)].

[35] Yu. F. Smirnov and Yu. I. Nechaev, Kinam 4, 445 (1982); Yu. I. Nechaev and Yu. F. Smirnov, Yad. Fiz. 35, 1385 (1982) [Sov. J. Nucl. Phys. 35, 808 (1982)].

[36] J. R. Bergervoet, P. C. van Campen, R. A. M. Klomp, J. L. de Kok, T. A. Rijken, V. G. J. Stoks and J. J. de Swart, Phys. Rev. C **41**, 1435 (1990).

[37] V. G. J. Stoks, R. A. M. Klomp, C. P. F. Terheggen and J. J. de Swart, Phys. Rev. C **49**, 2950 (1994).

[38] M. C. Birse, Phys. Rev. **C74**, 014003 (2006); Phys. Rev. **C76**, 034002 (2007); PoS **CD09**, 078 (2009).

[39] M. P. Valderrama, Phys. Rev. **C83**, 024003 (2011), Phys. Rev. **C84**, 064002 (2011).

[40] Bingwei Long and C. J. Yang, Phys. Rev. **C84**, 057001 (2011), Phys. Rev. **C85**, 034002 (2012), Phys. Rev. **C86**, 024001 (2012).

[41] Bingwei Long, Phys. Rev. C **88**, 014002 (2013).

[42] P. Navratil, J.P. Vary, B.R. Barrett, Phys. Rev. Lett. **84** (2000) 5728; Phys. Rev. C **62**, 054311 (2000).

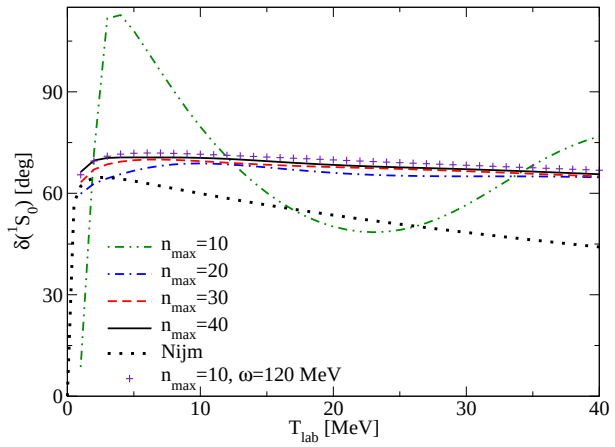

FIG. 1: ${}^1S_0$ LO phase shift as a function of laboratory energy $T_{lab} = 0 - 50$ MeV. Here the black-dot represent the Nijmegen phase shift, and each colored-line represents the phase shift with various n_{max}, where ω is fixed to 20 MeV except for the one with the "+" sign. Here the result is renormalized to give $a_0 = -23.7$ fm, and the potential has intrinsic cutoffs $\Lambda_c = 800$ MeV, $\Lambda = 600$ MeV.

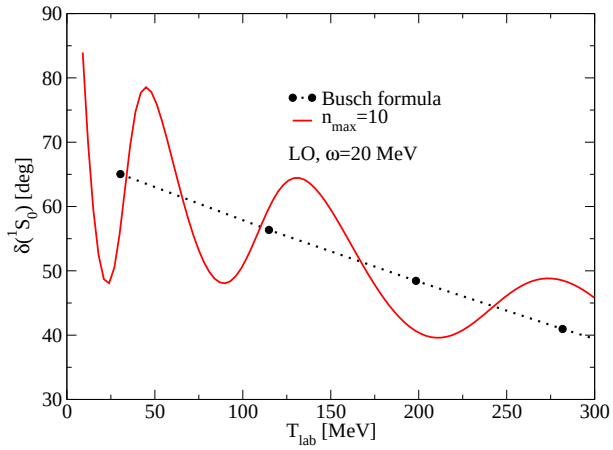

FIG. 2: $^1S_0$ LO phase shift as a function of laboratory energy $T_{lab} = 0 - 300$ MeV. Here the black circles represent phase shift obtained by Busch formula, and the red line represents the phase shift obtained by J-matrix method. Here $n_{max} = 10$, $\omega = 20$ MeV, and the potential has intrinsic cutoffs $\Lambda_c = 800$ MeV, $\Lambda = 600$ MeV.

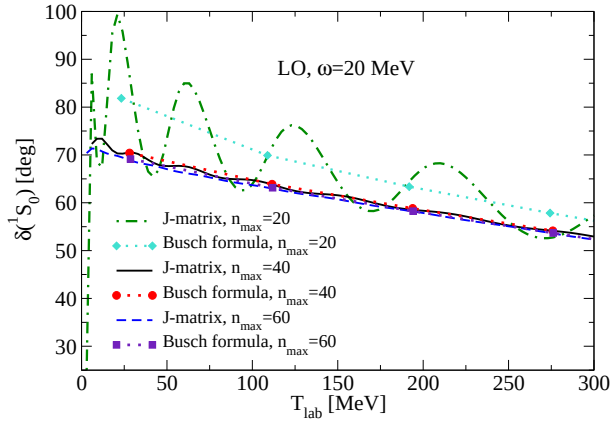

FIG. 3: $^1S_0$ LO phase shift as a function of laboratory energy $T_{lab} = 0-300$ MeV. Here phase shifts obtained by Busch formula (colored-symbol) are compared to those obtained by J-matrix method (colored-line). Here $n_{max} = 20, 40, 60$, and $\omega = 20$ MeV. The potential has intrinsic cutoffs $\Lambda_c = 1000$ MeV, $\Lambda = 800$ MeV.

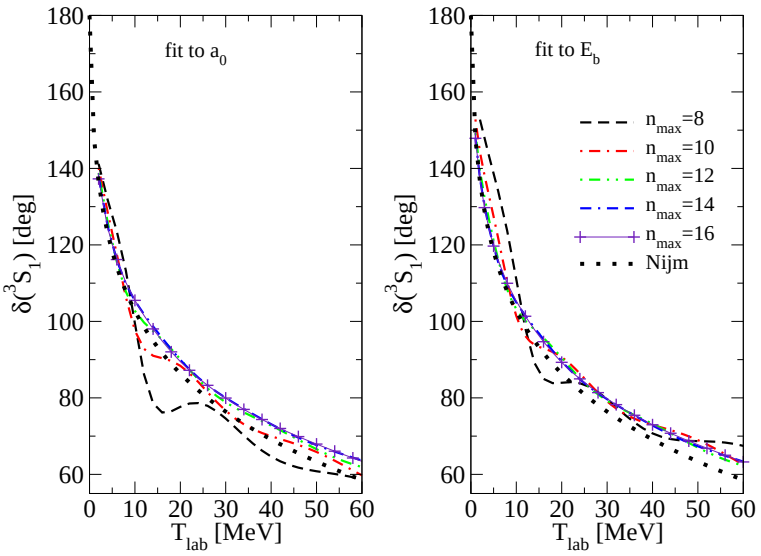

FIG. 4: ${}^3S_1$ LO phase shift as a function of laboratory energy $T_{lab} = 0 - 60$ MeV. Here the black-dot represent the Nijmegen phase shift, and each colored-line represents the phase shift with various n_{max}, where ω is fixed to 20 MeV. The LEC is renormalized to reproduce $a_0 = 5.4$ fm in the left panel, and is renormalized to reproduce the deuteron binding energy $E_b = -2.225$ MeV in the right panel. The potential has intrinsic cutoffs $\Lambda_c = 800$ MeV, $\Lambda = 600$ MeV.

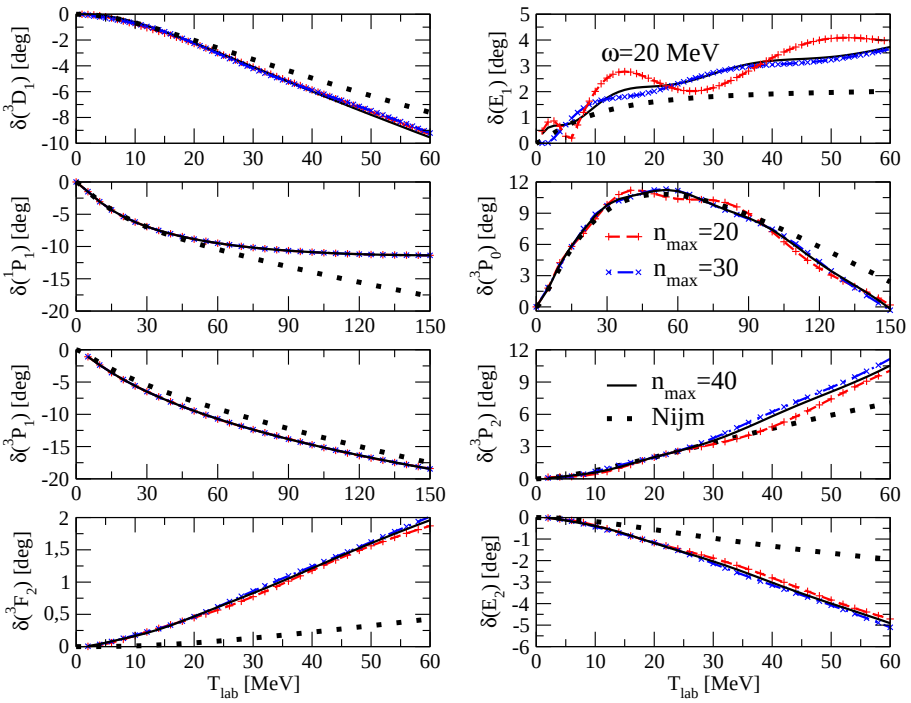

FIG. 5: Leading order phase shifts as a function of laboratory energy T_{lab}. Here the black-dot represent the Nijmegen phase shift, and each colored-line represents the phase shift with various n_{max}, where ω is fixed to 20 MeV, and the potential has intrinsic cutoffs $\Lambda_c = 800$ MeV, $\Lambda = 600$ MeV.

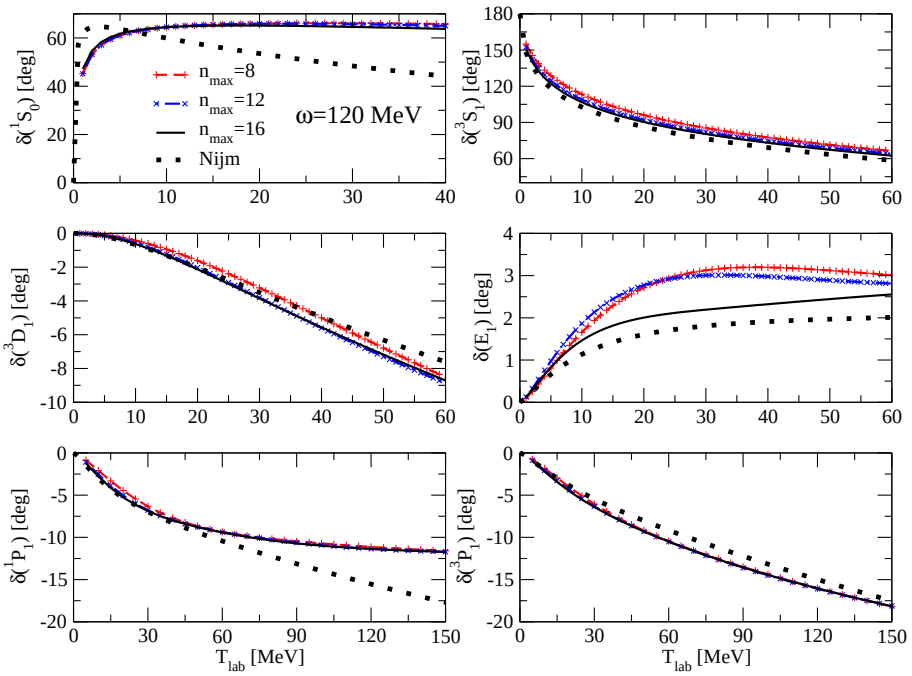

FIG. 6: Leading order phase shifts as a function of laboratory energy T_{lab}. Here the black-dot represent the Nijmegen phase shift, and each colored-line represents the phase shift with various n_{max}, where ω is fixed to 120 MeV, and the potential has intrinsic cutoffs $\Lambda_c = 1000$ MeV, $\Lambda = 800$ MeV.

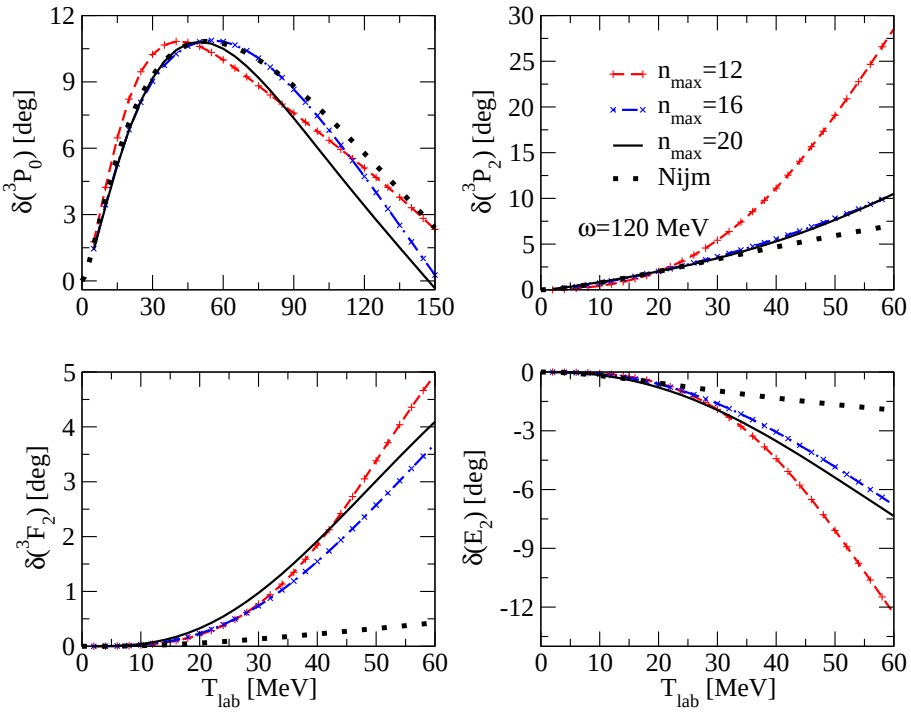

FIG. 7: Leading order phase shifts as a function of laboratory energy T_{lab}. Here the black-dot represent the Nijmegen phase shift, and each colored-line represents the phase shift with various N_{max}, where ω is fixed to 120 MeV, and the potential has intrinsic cutoffs $\Lambda_c = 1000$ MeV, $\Lambda = 800$ MeV.

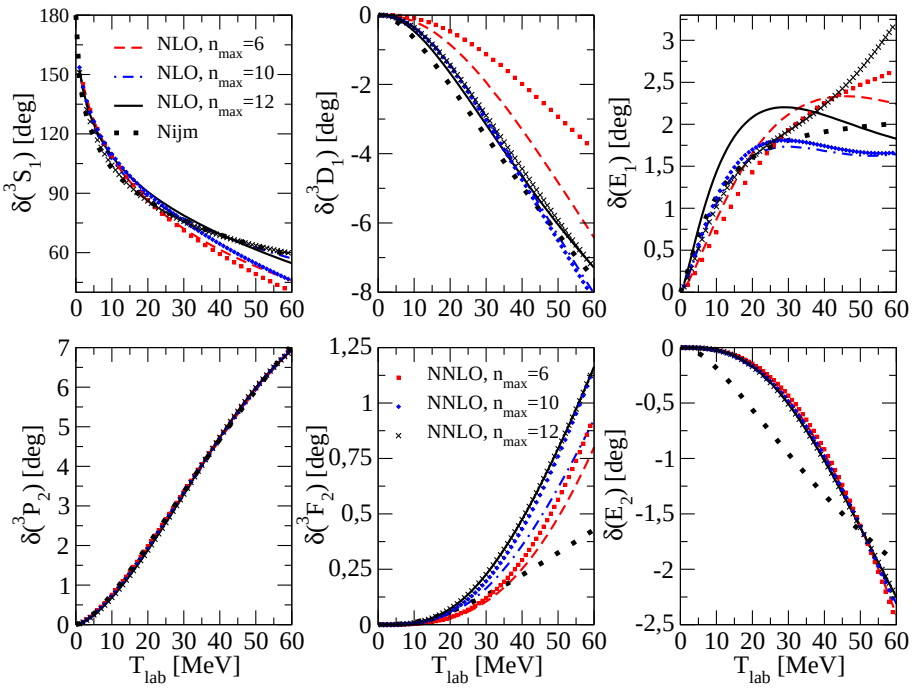

FIG. 8: NLO and NNLO coupled-channel phase shifts as a function of laboratory energy T_{lab}. Here the black-dot represent the Nijmegen phase shift, and each colored-line represents the phase shift with various n_{max}, where ω is fixed to 120 MeV and the intrinsic cutoffs are $\Lambda_c = 800$ MeV, $\Lambda = 600$ MeV.

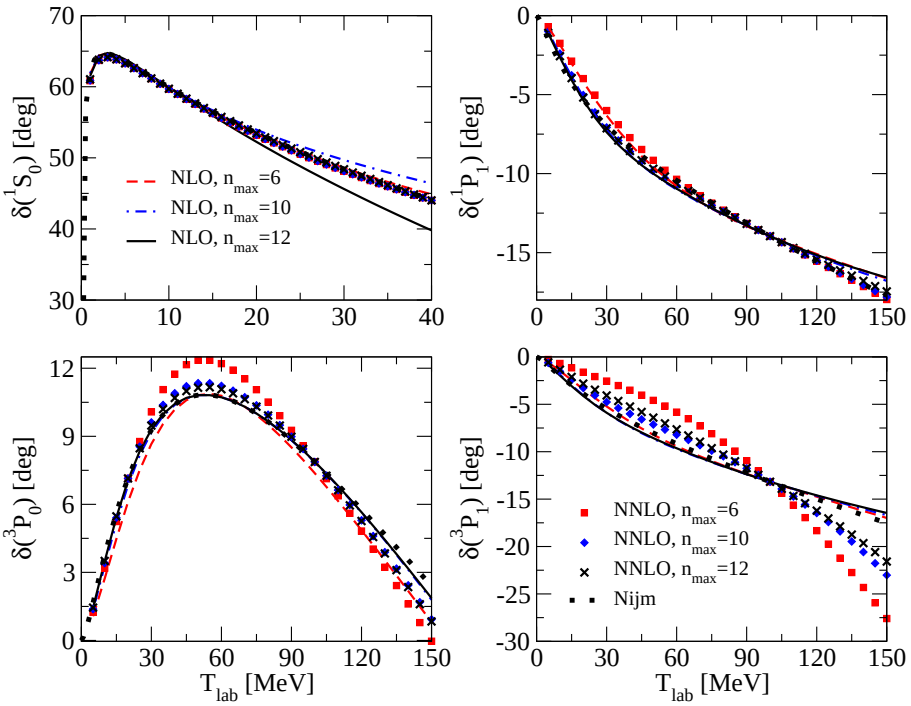

FIG. 9: NLO and NNLO uncoupled-channel phase shifts as a function of laboratory energy T_{lab}. Here the black-dot represent the Nijmegen phase shift, and each colored-line represents the phase shift with various n_{max}, where ω is fixed to 120 MeV and the intrinsic cutoffs are $\Lambda_c = 800$ MeV, $\Lambda = 600$ MeV.

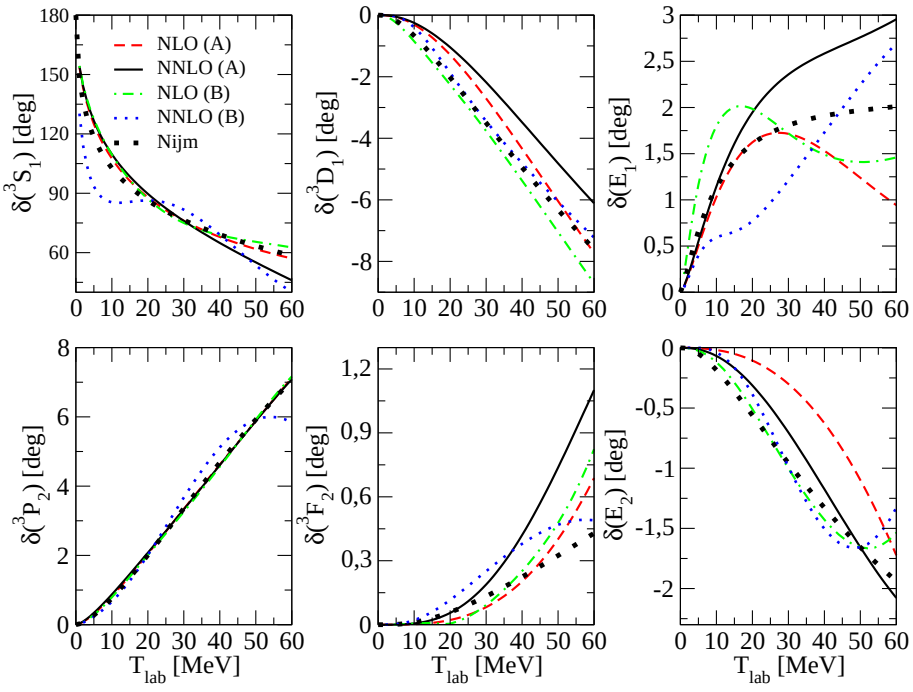

FIG. 10: NLO and NNLO coupled-channel phase shifts as a function of laboratory energy T_{lab}. Here the intrinsic cutoffs are $\Lambda_c = 1000$ MeV, $\Lambda = 800$ MeV, and black-dot represent the Nijmegen phase shift. Each colored-line represents the phase shift at various order and combination of (ω, n_{max}). Label (A) stands for (ω, n_{max})=(120 [MeV],8) for ${}^3S_1 - {}^3D_1$ channel and (120 [MeV],6) for ${}^3P_2 - {}^3F_2$ channel, and (B) stands for (ω, n_{max})=(60 [MeV],19) for ${}^3S_1 - {}^3D_1$ channel and (60 [MeV],15) for ${}^3P_2 - {}^3F_2$ channel.

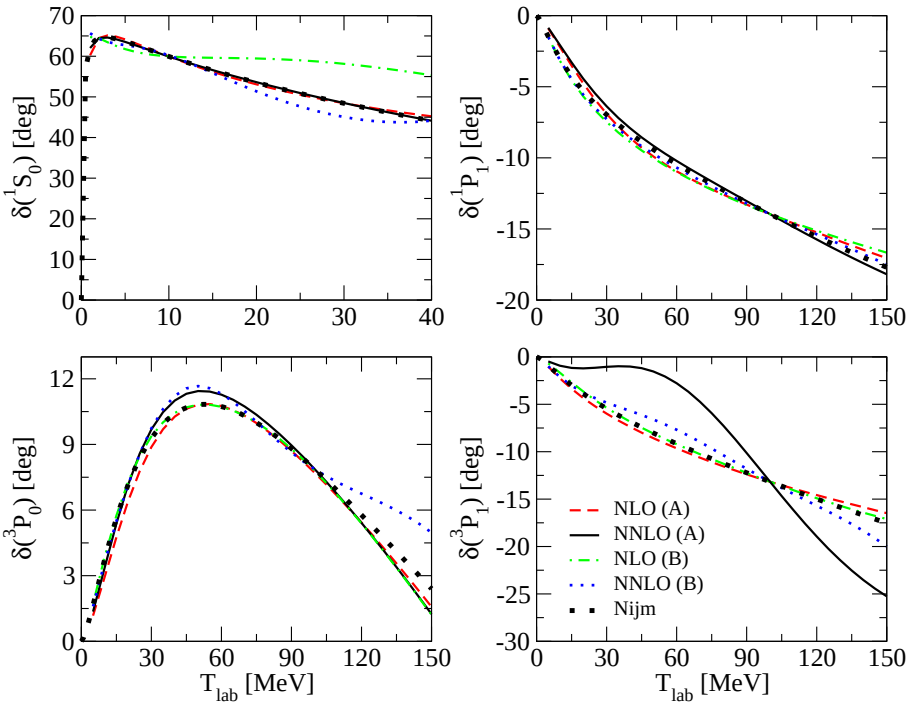

FIG. 11: NLO and NNLO uncoupled-channel phase shifts as a function of laboratory energy T_{lab}. Here the intrinsic cutoffs are $\Lambda_c = 1000$ MeV, $\Lambda = 800$ MeV, and black-dot represent the Nijmegen phase shift. Each colored-line represents the phase shift at various order and combination of (ω, n_{max}). Label (A) stands for (ω, n_{max})=(120 [MeV],8), and (B) stands for (ω, n_{max})=(60 [MeV],17).